Reconstruction of Finite Rate of Innovation Spherical Signals in the Presence of Noise Using Deep Learning Architecture

Muhammad Osama Tarar and Zubair Khalid
School of Science and Engineering, Lahore University of Management Sciences, Lahore, Pakistan 54792
osama.tarar@lums.edu.pk, zubair.khalid@lums.edu.pk

***Abstract*—We propose a method for the accurate reconstruction (recovery of parameters) of non-bandlimited finite rate of innovation (FRI) signals on the sphere from its measurements contaminated by additive isotropic noise. We propose a framework that takes the optimal number of noisy measurements and employs autoencoder (deep learning architecture) to enhance the signal consisting of a finite number of Diracs before estimating the parameters using the annihilating filter method. We use convolutional and fully connected autoencoders for signal enhancement in the spatial and spectral domains respectively. We analyse the denoising performance of both the overcomplete and undercomplete autoencoders and demonstrate the superior performance, measured as a gain in the signal to noise ratio (SNR) of the output signal, of the fully connected overcomplete autoencoder that filters the signal in the spectral domain. Through numerical experiments, we demonstrate the improvement enabled by the proposed framework in the accuracy of recovery of the parameters of the FRI signal.**

***Index Terms*—Finite rate of innovation, sphere, spherical harmonics, isotropic noise, autoencoders, deep learning**

I. Introduction

Spherical signals arise in many different fields of engineering and science such as medical imaging [1], geodesy [2], wireless communication [3], computer graphics [4], antenna theory [5], and acoustics [6]. To support signal analysis on the sphere in medical imaging, acoustics, and beyond, we consider the problem of signal reconstruction of non-bandlimited finite rate of innovation (FRI) signal, consisting of finite K number of Dirac delta functions, on the sphere from the noise-contaminated observations of the signal.

Different sampling techniques for the acquisition of spherical signals have been devised in recent years [7]. The spectral (harmonic) coefficients of the signal on the sphere are computed using the spherical harmonic transform (SHT) by taking a finite number of measurements on the sphere. SHT can be exactly computed assuming that the signal is bandlimited in the harmonic domain. Bandlimit existence is a powerful assumption and it has been used to devise sampling schemes (e.g., [7], [8]) on the sphere that supports exact/accurate signal reconstruction. These sampling schemes are however not suitable for non-bandlimited signals such as a stream of Diracs.

Z. Khalid is supported by Pakistan HEC TDF (Project no. 03-169).

An algorithm based on super-resolution theory has been developed in [9] for the recovery of parameters of FRI signals. However, the algorithm is iterative in nature and requires a minimum separation condition between the Diracs. Recently, signal processing techniques based on annihilating filter method (devised for Euclidean domain signals in [10], [11]) for the recovery of parameters of FRI signal on the sphere have been proposed [12]–[15]. [12] develops a method for the reconstruction of parameters of K Diracs that requires the samples of the signal bandlimit at degree (formally defined in Section 2.1) $L = 2K$. To reduce the number of samples by a factor of approximately four, an annihilating filter based algorithm has been proposed in [13]. However, the error in the recovery of parameters using these two methods increases with the number of Diracs due to the ill-conditioning of the linear systems used in the reconstruction. This problem has been addressed in [14], [15], where the annihilating filter method is also used for the development of algorithms that enable accurate recovery of the parameters of Diracs.In these methods, the measurements of the FRI signal are assumed to be free from any noise and/or distortions.

In this context, we consider the problem of estimation of the parameters of FRI signal (Diracs) from the measurements of the signal corrupted by additive isotropic noise. As we don't know the statistics of the signal corrupted by noise, we cannot use traditional spherical filtering techniques for denoising. We develop a framework that enhances (denoises) the observed signal using deep learning architectures and estimates the parameters of the Diracs using the annihilating filter method. Autoencoders have been used for denoising [16]–[20] as they outperform traditional denoising techniques and are not restrictive of noise generative processes. In the Euclidean setting, convolutional autoencoder performs better for images from their ability to exploit translational symmetries through weight sharing and translation equivariance. However, the autoencoders have not been used for denoising spherical signals and the focus has been on traditional spherical filters. We analyse the use of undercomplete/overcomplete fully connected (FC) and convolutional autoencoders (CAE) for enhancement of the signal in the spatial and spectral domains respectively. We train the architectures on the training data and analyse the signal to noise ratio (SNR) improvement provided by each of the autoencoders on testing data. We demonstrate

that the FC overcomplete autoencoder offers better denoising performance. We demonstrate that the proposed framework improves the accuracy of the recovered parameters of the FRI signal.

II. Problem Formulation

A. Mathematical Preliminaries – Signals on the Sphere

We define the unit sphere as $\mathbb{S}^2 \triangleq \{\hat{\boldsymbol{u}} \in \mathbb{R}^3 : |\hat{\boldsymbol{u}}| = 1\}$, where $|\cdot|$ refers to norm in the Euclidean space and $\hat{\boldsymbol{u}}$ is a vector of unit norm in $3D$ Euclidean domain $\mathbb{R}^3$ that represents the point on the 2-sphere (or sphere). A point $\hat{\boldsymbol{u}}$ on the sphere can be parameterized using two angles, referred to as colatitude θ and longitude ϕ, that is, $\hat{\boldsymbol{u}} \equiv \hat{\boldsymbol{u}}(\theta, \phi) = (\sin\theta\cos\phi, \sin\theta\sin\phi, \cos\theta)$, $\theta \in [0, \pi]$ is measured from the positive z axis and $\phi \in$ [0,2π) is measured from the positive x axis in the x-y plane. We define the inner product of two functions $f(\hat{\boldsymbol{u}})$ and $g(\hat{\boldsymbol{u}})$ as [21]

$$\langle f, g\rangle \triangleq \int_{\mathbb{S}^2} f(\hat{\boldsymbol{u}})\overline{g(\hat{\boldsymbol{u}})}ds(\hat{\boldsymbol{u}}), \tag{1}$$

where $ds(\hat{\boldsymbol{u}}) = \sin\theta d\theta d\phi$ is the differential element on $\mathbb{S}^2$, $\overline{(.)}$ denotes complex conjugate and the integration is carried out over the whole sphere. Complex valued functions on $\mathbb{S}^2$ form a Hilbert space $L^2(\mathbb{S}^2)$ equipped with the inner product defined in (1) which induces the norm $\| f \| \triangleq \langle f, f\rangle^{1/2}$.

The archetype complete orthonormal sequence for Hilbert space $L^2(\mathbb{S}^2)$ is the set of spherical harmonic functions, denoted by $Y_\ell^m(\hat{\boldsymbol{u}})$ for integer degree $\ell \geq 0$ and integer order $|m| \leq \ell$. Any signal $f \in L^2(\mathbb{S}^2)$ can be expanded in spherical harmonic functions as

$$f(\theta, \phi) = \sum_{\ell=0}^{\infty} \sum_{m=-\ell}^{\ell} (f)_\ell^m Y_\ell^m(\theta, \phi), \tag{2}$$

where $(f)_\ell^m$ is the spherical harmonic coefficient of degree ℓ and order m and is given by the spherical harmonic transform (SHT): $(f)_\ell^m \triangleq \langle f, Y_\ell^m\rangle$. The signal f is bandlimited at L if $(f)_\ell^m = 0, \forall\, \ell \geq L$.

B. Problem Formulation

We consider an ensemble of K Diracs located on the sphere corrupted by noise, that is,

$$y(\hat{\boldsymbol{u}}) = f(\hat{\boldsymbol{u}}) + n(\hat{\boldsymbol{u}}), \quad f(\hat{\boldsymbol{u}}) = \sum_{k=1}^{K} \alpha_k \delta(\hat{\boldsymbol{u}}, \hat{\boldsymbol{u}}_k) \tag{3}$$

where $\hat{\boldsymbol{u}}_k = \hat{\boldsymbol{u}}_k(\theta_k, \phi_k)$ indicates the location of k-th Dirac on the unit sphere, α_k denotes the complex amplitude, $n(\hat{\mathbf{u}})$ denotes the noise and $\delta(\hat{\mathbf{u}}, \hat{\mathbf{u}}_k)$ is the Dirac delta function that satisfies the sifting property given by $f(\hat{\boldsymbol{u}}_k) = \langle f, \delta(., \hat{\boldsymbol{u}}_k)\rangle$. We assume that the noise is isotropic and white, that is,

$$\mathbb{E}\{(n)_\ell^m \overline{(n)_p^q}\} = C\, \delta_{\ell p}\delta_{mq}, \tag{4}$$

where $\mathbb{E}$ is the expectation operator and $\delta_{\ell p}$ is the Kronecker delta function: $\delta_{\ell p} = 1$ for $\ell = p$ and is zero otherwise. The problem under consideration is to recover the parameters of the Diracs namely θ_k, ϕ_k and α_k as accurately as possible given the finite number of samples of bandlimited signal y.

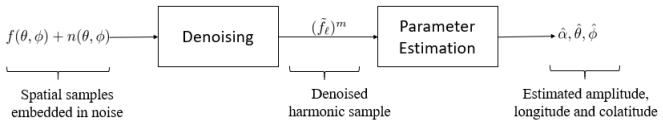

Fig. 1: The framework for the estimation of parameters of the Diracs from noise corrupted measurements.

III. Denoising and Estimation of Parameters

For the estimation of parameters of the signal f (ensemble of Diracs) formulated in (3) from the samples of the signal y bandlimited at degree L, we propose a framework (shown in Fig. 1) that employs the autoencoder architecture to denoise the signal before estimating the parameters. We analyse the performance of different autoencoders for denoising the signal.

A. Denoising using Autoencoders

We first require the signal to be denoised before the estimation of parameters. We assume that the signal is bandlimited at bandlimit L and the samples are taken over the equiangular sampling grid proposed in [8] for the exact reconstruction of bandlimited signals. We carry out denoising in both the spatial and spectral (constituted by spherical harmonic coefficients) domains. We employ SHT associated with the equiangular sampling scheme to compute the spherical harmonic coefficients. We analyse the performance of denoising experiments later in the paper.

Autoencoder is a type of neural network that is trained to learn to approximate the identity function [16]. Denoising utilizing autoencoders is carried out by using either fully connected or convolutional autoencoders [16]–[20]. Fully connected autoencoder encodes the input vector $\mathbf{x}$ into a latent space representation as vector $\mathbf{z}$ using a transformation of the form $\mathbf{z} = s(\mathbf{W}_c\mathbf{x} + \mathbf{b}_c)$, where s is a non-linear activation function, $\mathbf{W}_c$ is the weight matrix and $\mathbf{b}_c$ is the bias at the encoder. Latent space representation $\mathbf{z}$ is then decoded into an output space $\tilde{\mathbf{x}}$ having the same dimensionality as $\mathbf{x}$. This transformation also uses the similar mapping $\tilde{\mathbf{x}} = s(\mathbf{W}_d\mathbf{z} + \mathbf{b}_d)$. $(\mathbf{W}_c, \mathbf{W}_d, \mathbf{b}_c, \mathbf{b}_d)$ are the model parameters that need to be optimized so that the error in reconstruction is minimized. A convolutional autoencoder is similar to the fully connected autoencoder except that the transformation in the encoding and decoding layers is convolution operation.

Denoising autoencoder attempts to learn to reconstruct the input given that noisy measurements are fed at the input [16]. The autoencoders can be further classified into undercomplete if the dimension of the latent space is less than the dimension of input space. Otherwise, the autoencoders are referred to as overcomplete autoencoders. Since the encoded features are of higher dimension as compared to the input, overcomplete encoders offer better denoising performance as we demonstrate later in the next section.

B. Estimating Parameters

Next, we employ the annihilating filter method proposed in [15] to recover parameters. We use the denoised signal,

denoted by $\tilde{f}$ for the estimation of parameters. As indicated earlier, the samples are taken over the equiangular sampling scheme that enables the exact computation of spherical harmonic coefficients of the signal.

Making use of the sifting property, the spherical harmonic coefficients of the denoised signal can be approximately represented as $(\tilde{f})_l^m = \sum_{k=1}^{K} \alpha_k \overline{Y_\ell^m(\theta_k, \phi_k)} + (\tilde{n})_\ell^m$, where $\tilde{n}$ denotes the additive noise in the signal after denoising. Also, we note that $Y_\ell^m(\theta, \phi)$ can be written as $Y_\ell^m(\theta, \phi) = Y_\ell^m(\theta, 0)e^{-im\phi}$ and we can obtain $Y_\ell^m(\theta, 0)$ by multiplying with a polynomial in $\cos\theta$ which is of degree $(\ell - |m|)$ by $(\sin\theta)^{|m|}$ which is of degree $(|m|)$. In order to further expand the spherical harmonic coefficient expression of signal $\tilde{f}$, we denote the coefficients of polynomial in $\cos\theta$ by c_{lm}^p that corresponds to the polynomial in $\cos\theta_k^p$. We can now write the spherical harmonic coefficients for each order m as

$$(\tilde{f})_\ell^m = \sum_{k=1}^{K} \alpha_k \sum_{p=0}^{\ell-|m|} c_{\ell m}^p \big(\cos\theta_k\big)^p \big(\sin\theta_k\big)^{|m|} e^{-im\phi_k} + (\tilde{n})_\ell^m, \tag{5}$$

which we rearrange to express as

$$(\tilde{f})_\ell^m = \sum_{p=0}^{\ell-|m|} c_{\ell m}^p d_{pm} + (\tilde{n})_\ell^m, \tag{6}$$

where

$$d_{pm} = \begin{cases} \sum_{k=1}^{K} (\alpha_k y_{kp}) x_k^m & 0 \le m < L \\ \sum_{k=1}^{K} (\alpha_k y_{kp}) \overline{x_k^{-m}} & -L < m < 0 \end{cases} \tag{7}$$

Here $x_k = \sin\theta_k e^{-i\phi_k}$ and where $y_{kp} = (\cos\theta_k)^p$. Given the noise is isotropic and assuming that the autoencoder maintains the isotropic characteristics of the noise, we obtain d_{pm} for each m as least-squares estimate using the spherical harmonic coefficients $(\tilde{f})_\ell^m$ related to d_{pm} through (6). To obtain d_{pm}, we require the spherical harmonic coefficients to be computed $(\tilde{f})_\ell^m$ for all degrees $\ell \le L_{\max}$, $L_{\max} = K + \sqrt{K + \frac{1}{4}} - \frac{1}{2}$. We assume that the samples are taken on the equiangular scheme that supports the spherical harmonic coefficients up to degree $L > L_{\max}$. In (7), we note that d_{pm} for $0 \le m < L$ and $\overline{d_{pm}}$ for $-L < m < 0$ are made up of linear combinations of the exponentials x_k^m and therefore annihilating filter method [10] can be employed to recover these exponentials. Once we obtain the estimate of x_k, we compute the longitude parameters ϕ_k, $k = 1, 2, \ldots, K$ by taking the phase of x_k. Once the longitude parameters are estimated, the colatitude and amplitude parameters can be estimated by solving a system of linear equations given in (7) for $p = 1$ and $p = 0$ respectively (see [15]).

IV. Results and Analysis

We have the representation of the noise corrupted signal in both the spatial and spectral domains enabled by SHT. We, therefore, analyse the performance of both the fully connected and convolutional autoencoders for denoising in the spectral and spatial domains respectively.

1) Dataset: We prepare a dataset of Diracs for $K = 3$ and obtain the samples of the noisy signal on an equiangular sampling scheme for different values of $L \in \{8, 16, 32\}$. For each L and signal to noise ratio (SNR) defined as

$$\mathrm{SNR}^y = 10 \log_{10} \frac{\| f \|^2}{\| y - f \|^2}, \tag{8}$$

for signal y in the range $0 \le \mathrm{SNR}^y \le 20$ (dB), we generate $20,000$ data points, where each instance is obtained using (3) by randomly generating a noise of desired power and uniformly generating $\theta_k \in (0, \pi)$, $\phi_k \in [0, 2\pi)$ and α_k with real/imaginary parts distributed in $[-1, 1]$ for $k = 1, 2, \ldots, K$. We divide the data into 70% training instances and 30% test instances.

2) Autoencoder Architectures and Training: We made a fully connected autoencoder to denoise in the harmonic domain and a convolutional autoencoder to denoise in the spatial domain. Both types of autoencoders were four layers with a two-layer encoder and a two-layer decoder. Since the signal is complex in both the harmonic domain and spatial domain, we treat the real and imaginary parts of the signal as two real signals.

For fully connected (FC) autoencoder, we form the network with layers as FC-relu-FC-relu-FC-relu-FC. For the construction of an undercomplete autoencoder, the first encoder layer contains $L^2/2$ neurons and the second encoder layer contains $L^2/4$ neurons. $L^2/2$ neurons are present in the decoder first layer and L^2 neurons are present in the decoder second layer. The signal in the spectral domain which contains L^2 noisy harmonic coefficients is first encoded to $L^2/4$ latent space which in turn is decoded back to L^2 reconstructed harmonic coefficients. For overcomplete autoencoder, the first encoder layer contains L^2 neurons and the second encoder layer contains $2L^2$ neurons. L^2 neurons are present in the decoder first layer and L^2 neurons are present in the decoder second layer. The signal in the spectral domain which contains L^2 noisy harmonic coefficients is first encoded to $2L^2$ latent space which in turn is decoded back to L^2 reconstructed harmonic coefficients. In the overcomplete autoencoder, there are many more parameters to be optimized and therefore there is a tradeoff between the denoising performance and the number of parameters. For example, the undercomplete autoencoder for $L = 8$ has approximately 5000 parameters to be optimized compared to approximately 25000 parameters of the overcomplete autoencoder.

For convolutional autoencoder (CAE), the undercomplete autoencoder contains the layers as conv$2D$-relu-maxpool$2D$-conv$2D$-relu-maxpool$2D$-conv$2D$-relu-upsampling$2D$-conv$2D$-relu- upsampling -$2D$-conv$2D$. The filters are of size 3×3 with the number of filters 16, 32, 32, 16 and 8 respectively and a stride of 1. The zero paddings are done such that the convolution layer operation does not change the dimension of its input. Only the maxpool$2D$ layer reduces the dimension by a factor of two and upsampling$2D$ increases the dimension

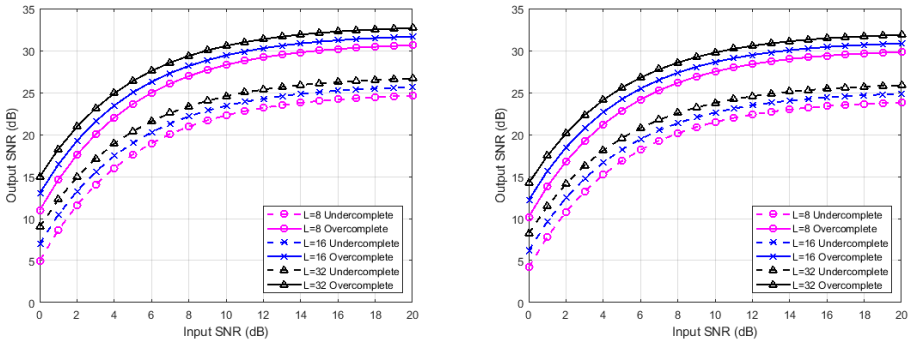

(a) (b)

Fig. 2: Output $\text{SNR}^{\tilde{f}}$ against the input SNR^{y} for bandlimit $L \in \{8, 12, 16\}$ and (a) fully connected overcomplete and undercomplete autoencodder and (b) convolutional overcomplete and undercomplete autoencodder.

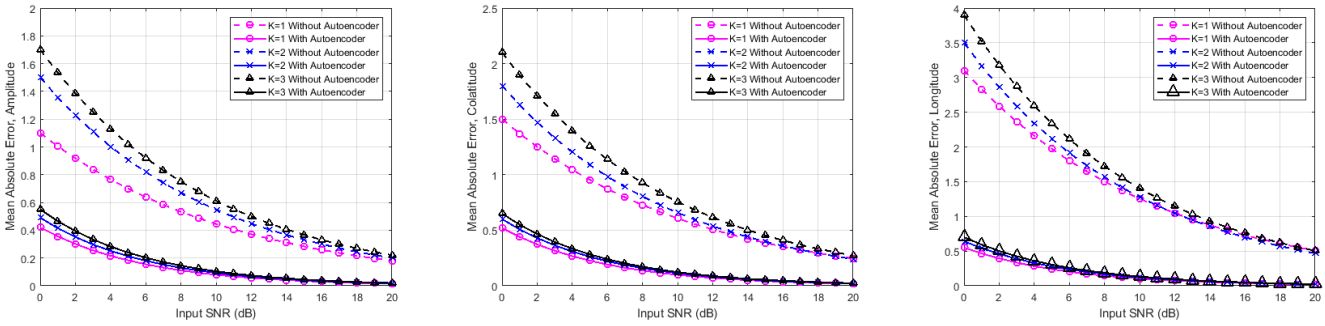

(a) (b) (c)

Fig. 3: Mean Absolute Error of the recovered (a) Amplitude α, (b) Colatitude θ and (c) Longitude ϕ against input SNR^{y} for $K = 1, 2$ and 3, with and without the use of FC overcomplete autoencoder for denoising.

by a factor of two. Overall, the noisy signal in the spatial domain of size $2L \times 2L$ is first encoded to $L/2 \times L/2$ latent space which in turn is decoded back to $2L \times 2L$ reconstructed spatial signal. The overcomplete autoencoder contains the layers as conv$2D$-relu-conv$2D$-relu-upsampling$2D$-conv$2D$-relu-maxpool$2D$-conv$2D$-relu-conv$2D$. Again the number of filters is 16, 32, 32, 16, and 8 respectively, and are of size 3×3 with a stride of 1 and zero paddings ensure no change in the dimension in the convolution layer. Now the noisy signal in the spatial domain of size $2L \times 2L$ is first encoded to $4L \times 4L$ latent space and decoded back to $2L \times 2L$ reconstructed spatial signal.

3) Training and Performance Analysis: We train the autoencoders using the training data at a particular SNR. During the training, the resulting output for each input is used to compute the reconstruction error $\| \tilde{f} - f \|^2$, which is used to optimize the parameters of the autoencoders. We use RMSprop as the optimizer and train each network for 50 epochs.

Once the networks are trained, we use testing data to analyse the performance for each of the autoencoders under consideration. For each instance of the testing data, we compute the output SNR to quantify the improvement enabled by the autoencoders. We plot output $\text{SNR}^{\tilde{f}}$ against input SNR^{y} averaged over all the instances of the testing data for FC and CAE autoencoders in Fig. 2(a) and (b) respectively, where it can be observed that the filtering in the harmonic domain using the FC autoencoder outperforms the denoising in the spatial domain using the CAE encoder. We note that the improved performance is not due to overfitting since it is measured on the testing data. Furthermore, the analysis reveals that the improvement increases with the bandlimit and overcomplete autoencoder, in comparison to the undercomplete encoder, offers more improvement in the output SNR.

4) Relationship between the number of encoding layers, number of Diracs K and input SNR: Since FC overcomplete autoencoder outperforms the other choices, we use it to study the relationship between the number of encoding layers, the number of Diracs K, and input SNR. We first study the effect of using a different number of encoding layers for a constant K and varying input SNR. In the other experiment, we study the effect of using different encoding layers for a constant input SNR and varying K. The network is symmetric and we use a maximum of 5 encoder layers. For $K = 3$, output SNR is plotted against the number of layers for input SNR of 0 dB, 5 dB, and 10 dB in Fig. 4, where it can be observed that the performance increases with the increase in the number of encoding layers. For input SNR$= 0$ dB, we compute the output SNR against the number of layers for different number of Diracs $K = 3$,$K = 6$ and $K = 9$ and plot in Fig. 4, where it is evident that the number of encoding layers proportional to the number of Diracs improves the performance of signal reconstruction.

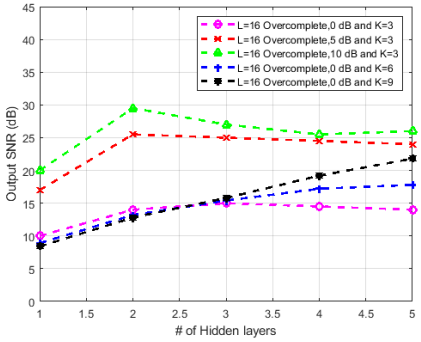

Fig. 4: Relationship between the number of encoding layers, number of Diracs K and input SNR

5) Parameter Estimation using the Optimal Number of Samples: Now, we will employ the annihilating filter method technique to recover the parameters (amplitude, colatitude, and longitude) of Diracs on the sphere. We analyse the improvement in the accuracy of the recovered parameters due to the signal enhancement offered by the proposed denoising framework.

We construct the Diracs dataset for $K = 1, 2$ and 3. However, we generate the dataset this time by taking the optimal number of samples as required for FRI parameter estimation [15]. We take band-limit $L = 2$, 3, and 5 for $K = 1$, 2, and 3, respectively. For signal enhancement, we construct FC overcomplete autoencoder with layers structured as FC-relu-FC-relu-FC-relu-FC. The first encoder layer contains $2L^2$ neurons and the second encoder layer contains $4L^2$ neurons. $2L^2$ neurons are present in the decoder first layer and L^2 neurons are present in the decoder second layer. This structure requires approximately 350, $1,700$ and $12,700$ parameters to be optimized for $L = 2$, 3 and 5, respectively. We estimate the parameters of the Diracs and plot the mean absolute error in the recovery of amplitudes, colatitudes, and longitudes in Fig. 3(a), (b) and (c) respectively, where it is evident that the proposed framework enables improvement in the accuracy of the recovery of the Diracs.

V. Conclusions

In this work, we have proposed a method for the accurate reconstruction of an FRI signal consisting of K Dirac functions on the sphere in the presence of noise. We have presented a framework that denoises the signal using deep learning architecture called autoencoder followed by the estimation of the parameters of the signal using the annihilating filter technique. We have analysed the use of different autoencoders for the signal enhancement in the presence of noise and demonstrated that FC overcomplete autoencoder provides the best improvement in the signal to noise ratio of the filtered signal. Using the trained network, we have also estimated the parameters of the Diracs and shown that the proposed framework improves the accuracy of the recovery of parameters. We have assumed the isotropic noise process in this work. We consider the analysis of the proposed framework for the recovery of parameters of the FRI signal corrupted by anisotropic noise as future work.

References

[1] Alice P. Bates, Z. Khalid, and R. A. Kennedy, "An optimal dimensionality sampling scheme on the sphere with accurate and efficient spherical harmonic transform for diffusion mri," *IEEE Signal Process. Lett.*, vol. 23, no. 1, pp. 15–19, Jan. 2016.

[2] Frederik J Simons and FA Dahlen, "Spherical slepian functions and the polar gap in geodesy," *Geophys. J. Int.*, vol. 166, no. 3, pp. 1039–1061, 2006.

[3] Y. F. Alem, Zubair Khalid, and R. A. Kennedy, "3d spatial fading correlation for uniform angle of arrival distribution," *IEEE Commun. Lett.*, vol. 19, no. 6, pp. 1073–1076, June 2015.

[4] Saad Nadeem, Zhengyu Su, Wei Zeng, Arie Kaufman, and Xianfeng Gu, "Spherical parameterization balancing angle and area distortions," *IEEE transactions on visualization and computer graphics*, vol. 23, no. 6, pp. 1663–1676, 2016.

[5] Rajavardhan Talashila and Harishankar Ramachandran, "Determination of far fields of wire antennas on a pec sphere using spherical harmonic expansion," *IEEE Antennas and Wireless Propagation Letters*, vol. 18, no. 4, pp. 646–650, 2019.

[6] H. Liu, Y. Fang, and Q. Huang, "Efficient representation of head-related transfer functions with combination of spherical harmonics and spherical wavelets," *IEEE Access*, vol. 7, pp. 78214–78222, June 2019.

[7] Z. Khalid, R. A. Kennedy, and J. D. McEwen, "An optimal-dimensionality sampling scheme on the sphere with fast spherical harmonic transforms," *IEEE Trans. Signal Process.*, vol. 62, no. 17, pp. 4597–4610, Sept. 2014.

[8] J. D. McEwen and Y. Wiaux, "A novel sampling theorem on the sphere," *IEEE Trans. Signal Process.*, vol. 59, no. 12, pp. 5876–5887, Dec. 2011.

[9] T. Bendory, S. Dekel, and A. Feuer, "Super-resolution on the sphere using convex optimization," *IEEE Trans. Signal Process*, vol. 63, no. 9, pp. 2253–2262, May 2015.

[10] M. Vetterli, P. Marziliano, and T. Blu, "Sampling signals with finite rate of innovation," *IEEE Trans. Signal Process*, vol. 50, no. 6, pp. 1417–1428, 2002.

[11] P. Shukla and P. L. Dragotti, "Sampling schemes for multidimensional signals with finite rate of innovation," *IEEE Trans. Signal Process*, vol. 55, no. 7, pp. 3670–3686, 2007.

[12] S. Deslauriers-Gauthier and P. Marziliano, "Sampling signals with a finite rate of innovation on the sphere," *IEEE Trans. Signal Process*, vol. 61, no. 18, pp. 4552–4561, 2013.

[13] I. Dokmanic and Y. M. Lu, "Sampling sparse signals on the sphere: Algorithms and applications," *IEEE Trans. Signal Process*, vol. 64, no. 1, pp. 189–202, 2016.

[14] Y. Sattar, Z. Khalid, and R. A. Kennedy, "Robust reconstruction of spherical signals with finite rate of innovation," *IEEE International Conference on Acoustics, Speech and Signal Processing (ICASSP)*, pp. 4024–4028, 2017.

[15] Y. Sattar, Z. Khalid, and R. A. Kennedy, "Accurate reconstruction of finite rate of innovation signals on the sphere," *IEEE International Conference on Acoustics, Speech and Signal Processing (ICASSP)*, pp. 1727–1731, 2019.

[16] L. Gondara, "Medical image denoising using convolutional denoising autoencoders," *In Proc. ICDMW*, pp. 241–246, 2016.

[17] Zhuoqun Fang, Tong Jia, Qiusheng Chen, Ming Xu, Xi Yuan, and Chengdong Wu, "Laser stripe image denoising using convolutional autoencoder," *Results in Physics, ELSEVIER*, pp. 96–104, 2018.

[18] Hsin-Tien Chiang, Yi-Yen Hsieh, Szu-Wei Fu, Kuo-Hsuan Hung, Yu Tsao, and Shao-Yi Chien, "Noise reduction in ecg signals using fully convolutional denoising autoencoders," *IEEE Access*, vol. 7, pp. 60806–60813, 01 2019.

[19] Xingchen Liu, Qicai Zhou, Jiong Zhao, Hehong Shen, and Xiaolei Xiong, "Fault diagnosis of rotating machinery under noisy environment conditions based on a 1-d convolutional autoencoder and 1-d convolutional neural network.," *Sensors*, pp. 19(4), 972, 2019.

[20] Peng Xiong, Hongrui Wang, Ming Liu, Suiping Zhou, Zengguang Hou, and Xiuling Liu, "Ecg signal enhancement based on improved denoising auto-encoder," *Engineering Applications of Artificial Intelligence*, vol. 52, pp. 194–202, 2016.

[21] R. A. Kennedy and P. Sadeghi, *Hilbert Space Methods in Signal Processing*, Cambridge University Press, Cambridge, UK, Mar. 2013.